

Order-disorder transitions to 2×2 structures

J. S. Walker

*Department of Physics, University of Pennsylvania,
Philadelphia, Pennsylvania 19104*

M. Schick

*Department of Physics, University of Washington, Seattle, Washington 98195
(Received 7 May 1979)*

We study the transitions to 2×2 ordered states which can occur in the triangular and honeycomb lattice gases with first- and second-neighbor repulsions only. A simple renormalization group which preserves the symmetry of such states, but not that of the $(\sqrt{3} \times \sqrt{3}) R 30^\circ$ phase, is employed. We find that the 2×2 phases exist in a very narrow region of density. In addition to phase diagrams, specific heats are calculated.

I. INTRODUCTION

There has been considerable activity recently, both experimental and theoretical, in the area of order-disorder transitions on surfaces.¹⁻⁷ Such transitions are attractive experimentally because they occur in a multitude of physisorbed and chemisorbed systems and can be studied by numerous techniques. They are also of theoretical interest for several reasons. In physisorbed systems in which the interactions are of short range, the transitions are thought to be in universality classes which have been of particular interest.¹ A case in point is the transition to a $(\sqrt{3} \times \sqrt{3}) R 30^\circ$ structure which occurs in systems adsorbed on a triangular lattice for a certain range of interaction parameters. This transition is predicted² to be in the class of the three-state Potts model, a prediction which has received experimental support.^{3,4} Several theoretical calculations of the properties of these systems have been carried out by various methods and for various interaction strengths with considerable agreement between theory and experiment.⁵⁻⁷ In chemisorbed systems, the determination of critical exponents is more complicated both theoretically and experimentally: theoretically because the presence of long-range forces⁸ will cause the exponents to change from their short-range values to (unknown) long-range values within some (unknown) region near the critical temperature⁹; experimentally because the limited coherence of present electron beams precludes the determination of exponents by low-energy electron diffraction (LEED), the usual probe. However, calculation of the phase diagram permits a determination of the values of the short-range interactions which are of considerable interest.

A transition which is of particular interest for both physisorbed and chemisorbed systems is that to a

2×2 structure on substrates which present either a triangular or honeycomb array of adsorption sites. This transition has been predicted¹⁰ to be in the universality class of the four-state Potts model whose critical exponents are believed to be known. Experiments on physisorbed systems which undergo such a transition would therefore be of great interest. Two chemisorbed systems which undergo this transition, O on Ni(111),¹¹ and H on Ni(111),¹² have recently been studied permitting interaction strengths to be extracted.

In this paper we calculate the phase diagram and specific heat of a system which exhibits the 2×2 transition; the triangular lattice gas with repulsive first- and second-neighbor interactions. The 2×2 transition on the honeycomb lattice is also studied. Section II is devoted to the triangular case. Qualitative features of the phase diagram which can be expected from ground-state energy arguments and consideration of symmetry are presented in Sec. II A. In Sec. II B the approximate renormalization-group methods we employ are discussed and in Sec. II C the results are presented. The 2×2 transition on the honeycomb lattice is discussed in Sec. III. We conclude with a brief summary.

II. TRIANGULAR LATTICE GAS WITH FIRST- AND SECOND-NEIGHBOR REPULSION

A. Expected phase diagram

We consider a two-dimensional gas of atoms which are restricted to a triangular lattice. They interact with a repulsion of strength u_1 , u_2 between first- and second-neighbors, respectively. A chemical potential μ determines the density n . As is well known, such a lattice gas is isomorphic to an Ising model with re-

duced Hamiltonian

$$-\beta\mathcal{H} = K \sum_{\langle ij \rangle} S_i S_j + L \sum_{\langle\langle ij \rangle\rangle} S_i S_j + H \sum_i S_i + NC, \quad S_i = \pm 1, \quad (2.1)$$

where the first and second sums are over nearest- and second-nearest-neighbor interactions, respectively. In addition K and L , which are negative (antiferromagnetic), are given by $K = -\frac{1}{4}\beta u_1$, $L = -\frac{1}{4}\beta u_2$. Also

$$H = \frac{1}{2} [\beta\mu - 3\beta(u_1 + u_2) - \ln\lambda_T^2/v_0]$$

and

$$C = \frac{1}{2} [\beta\mu - \frac{3}{2}\beta(u_1 + u_2) - \ln\lambda_T^2/v_0],$$

where λ_T and v_0 are the thermal wavelength and area of the primitive cell of the substrate, respectively. Thus we have a spin system with first- and second-neighbor antiferromagnetic interactions in the presence of a magnetic field.

Several aspects of the phase diagram can be established from a combination of ground-state energy arguments and the Landau-Lifshitz theory of second-order phase transitions. As we are interested in physical applications we restrict our attention to the regime for which the ratio $L/K \equiv a$ does not exceed unity.

Consider the ground state. It is clear from the nature of the interactions that there are only four kinds of ground state to be considered; (i) the paramagnetic phase, (ii) the 2 × 2 phase shown in Fig. 1(a), (iii) the $(\sqrt{3} \times \sqrt{3}) R 30^\circ$ phase of Fig. 1(b), and (iv) the 2 × 1 phase of Fig. 1(c). A comparison of the

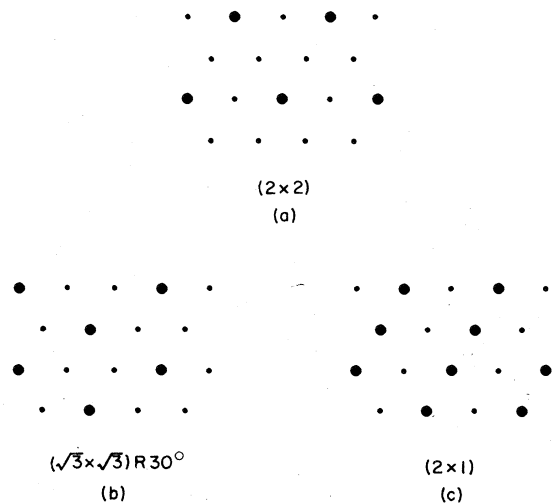


FIG. 1. Three ordered ground states which can be obtained with repulsive first- and second-neighbor interactions: (a) 2 × 2, (b) $(\sqrt{3} \times \sqrt{3}) R 30^\circ$, (c) 2 × 1.

ground-state energies of the three ordered phases and the paramagnetic phase at zero temperature yields the following information:

For $1 \geq a > \frac{1}{5}$ (a) the 2 × 1 phase exists for $|H/K| < 2(1+a)$, (b) the $(\sqrt{3} \times \sqrt{3}) R 30^\circ$ phase does not exist at $T=0$, (c) the 2 × 2 phase exists for $2(1+a) < |H/K| < 6(1+a)$. For $\frac{1}{5} \geq a$, (a) the 2 × 1 phase exists for $|H/K| < 12a$, (b) the $(\sqrt{3} \times \sqrt{3}) R 30^\circ$ phase exists for $12a < |H/K| < 6(1-3a)$, (c) the 2 × 2 phase exists for $6(1-3a) < |H/K| < 6(1+a)$.

Additional information is obtained from the Landau-Lifshitz¹³ theory of second-order phase transitions. As details of the analysis have been presented elsewhere,¹ we simply quote the results. The 2 × 1 states can be reached by a continuous transition from the disordered system only for $H=0$. At this point the transition is in the class of the Heisenberg model with cubic anisotropy. At nonzero field continuous transitions from the disordered system are to a 2 × 2 state and in the class of the four-state Potts model.

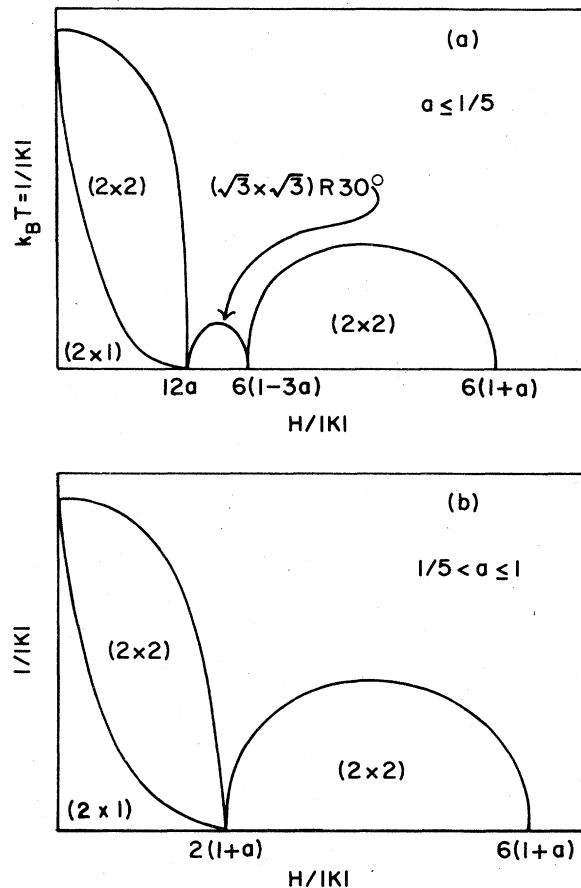


FIG. 2. Schematic phase diagram for two ranges of a , the ratio of the second- to first-neighbor repulsions: (a) a less than $\frac{1}{5}$, (b) a between $\frac{1}{5}$ and 1.

Transitions from 2×2 to 2×1 symmetry can be continuous and are in the class of the ferromagnetic Ising model. Where transitions from the disordered to the $(\sqrt{3} \times \sqrt{3})$ $R30^\circ$ phase occur, they are in the class of the three-state Potts model. The above information leads to the schematic phase diagram of Fig. 2, which is symmetric about $H=0$. Of note is the lens-shaped region of 2×2 symmetry at lower temperatures. The reader should not envisage that the particular 2×2 state shown in Fig. 1(a), and which represents the 2×2 ground state which exists at zero temperature for a finite region of H , is a good representation of the system in the lens-shaped region. Instead consider the most general state of 2×2 symmetry shown in Fig. 3, in which lattice-gas occupations on identically labelled sites are the same. The particular state of Fig. 1(a) corresponds to the special case $A = B = C \neq D$ or one of its permutations. In the lens-shaped region we expect the occupations to be almost equal in pairs; $A \approx B \neq C \approx D$ for example. The reason is that this state can make a continuous transition to the 2×1 state which corresponds to the special case $A = B \neq C = D$ or permutations thereof.

The difference between the two 2×2 states can be easily formulated in terms of the Landau-Ginsburg-Wilson Hamiltonian which describes the transition to the ordered state characterized by a three-component order parameter ψ_i ($i=1, 2, 3$). This Hamiltonian is, to fourth order in ψ ,

$$H_{\text{LGW}} = r \sum_i \psi_i^2 + \sum_i (\nabla \psi_i)^2 + u \psi_1 \psi_2 \psi_3 + w (\sum_i \psi_i^2)^2 + v \sum_i \psi_i^4.$$

Just below the transition the largest anisotropic term is the cubic term which, for $u \neq 0$, favors a 2×2 state for which $|\psi_1| = |\psi_2| = |\psi_3|$. This corresponds to three sublattices being equally occupied. As the temperature is lowered, the anisotropic fourth-order term must be considered. If v is negative, this term also

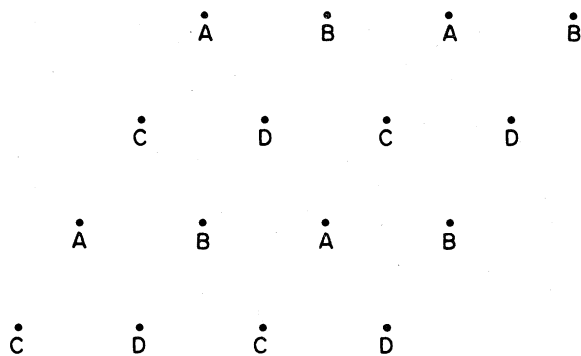


FIG. 3. Most general labeling of a 2×2 state. Lattice-gas occupations of identically labeled sites are the same.

favors the state in which three sublattices are equally occupied and the ground state of Fig. 1(a) will ultimately be reached. If v is positive however, this term favors the state $|\psi_1| = |\psi_2| = 0, \psi_3 \neq 0$, which is in fact a state of 2×1 symmetry. In the lens-shaped region, the terms in u and v are in competition.

It should be noted that the ground-state energy arguments cannot identify any phases which exist solely above some finite temperature. For example there is no $(\sqrt{3} \times \sqrt{3})$ $R30^\circ$ ground state for $L/K > \frac{1}{5}$. It is conceivable, however, that this phase could be stable at finite temperatures. This could also be the case for other ordered phases. Thus it must be recognized that the information obtained in this section is not necessarily complete.

B. Approximate renormalization-group calculation

We now develop a position-space renormalization-group (RG) calculation appropriate to the study of the Hamiltonian of Eq. (2.1). In a previous publication⁵ we have studied the transition to the $(\sqrt{3} \times \sqrt{3})$ $R30^\circ$ phase for the case of $L=0$, using a renormalization-group calculation based on dividing the original triangular lattice of adsorption sites into three separate sublattices. To study the 2×2 and 2×1 ordered phases, represented in Figs. 1(a) and 1(c), it can be seen that a division of the lattice into four sublattices is appropriate. This is illustrated in Fig. 4. In what follows, we shall confine our attention mainly to the transition leading to the 2×2 and

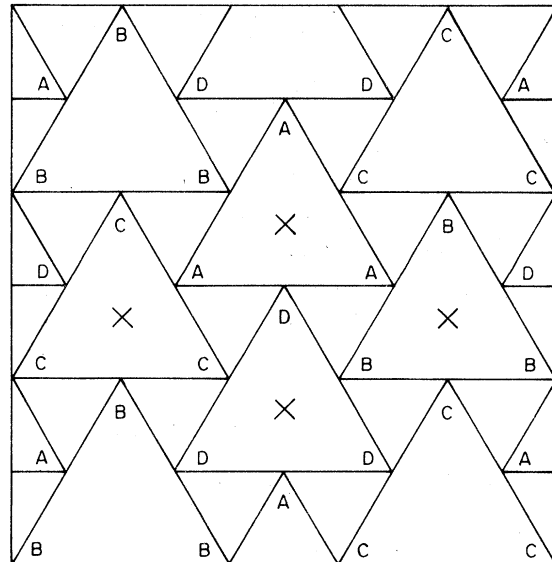


FIG. 4. Division of sites into cells. Each cell contains three sites from one sublattice only. Crosses denote four different cells used in the renormalization group.

2×1 phases, and thus a four sublattice formulation of the problem shall be employed, even though the $(\sqrt{3} \times \sqrt{3}) R 30^\circ$ structure cannot be adequately described in such a manner.

Once the lattice has been divided into sublattices appropriate to describe the ordered phases of interest, one must then choose a suitable grouping of lattice sites to form cells. As has been demonstrated in previous calculations,^{5,14} it is crucial that the choice of cells reflect the underlying symmetries of interest in the system. Foremost among these, in the present case, is the requirement that the four sublattice symmetry, which is essential in describing the 2×2 and 2×1 ordered states, be maintained under the renormalization-group transformation. Thus, if the initial state of the system is one of the possible 2×2 states, a state in which only the A sites are occupied, for example, then one must guarantee that this state will be mapped onto a renormalized system in which, again, only A sites are filled. With complete symmetry in the way the A , B , C , and D sublattices are treated, all possible 2×2 and 2×1 states will be thus preserved. The cells shown in Fig. 4, each of which consists of three-site spins chosen from a single sublattice, will clearly preserve the sublattice symmetry. The RG described here consists of choosing one of these cells from each of the four sublattices (e.g., those cells marked with an \times in Fig. 4) so that each sublattice is treated equivalently. Thus a total of 12 spins are considered. Note that while the above choice has been designed to preserve the 2×2 and 2×1 states, it fails to preserve the $(\sqrt{3} \times \sqrt{3}) R 30^\circ$ states since these cannot be represented in terms of four sublattices. In fact, a system initially in a $(\sqrt{3} \times \sqrt{3}) R 30^\circ$ state will be mapped to a paramagnetic state on the first iteration of this RG. Only a larger calculation, involving more sublattices and more cells, can simultaneously preserve the 2×2 , 2×1 , and $(\sqrt{3} \times \sqrt{3}) R 20^\circ$ ordered states.

We now study the four cells chosen above by employing the cell-cluster method of Niemeijer and van Leeuwen,¹⁵ together with the standard majority-rule projection of site spins to cell spins. Also, the 12 spins we consider are taken to be periodically extend-

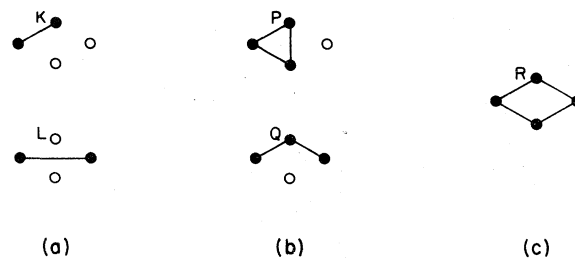


FIG. 5. Interactions which are propagated by the renormalization group. Two-spin, three-spin, and four-spin interactions are shown in (a), (b), and (c).

ed over the entire lattice, and the cell spins, similarly, will be treated periodically. This choice of periodic boundary conditions will guarantee that the correct zero-temperature behavior, as depicted in Fig. 2(b), will result. As the transformation does not preserve the $(\sqrt{3} \times \sqrt{3}) R 30^\circ$ state, its phase boundaries at zero temperature will not be obtained.

As is generally the case with RG transformations, additional interaction parameters, not present in the original Hamiltonian, will be generated under iteration of the group. These additional interactions will include interactions among all possible subsets of the cells which define the RG. Since, in this case, the RG is defined in terms of four cells, it is possible to generate interactions coupling zero, one, two, three, and four spins at a time. The zero-spin interaction is simply the constant term which contributes to the free energy, while the single-spin interaction is the magnetic field. The possible two-, three-, and four-spin interactions are shown in Fig. 5. Note that the four cell spins form a diamond-shaped configuration, and the possible interactions are represented by the solid lines. Two-spin interactions can connect nearest- or next-nearest neighbors and these interactions are designated by K and L , respectively. Three-spin interactions can be of two types, labeled P and Q , and the four-spin interaction, R , couples all four spins in the diamond-shaped figure. Thus the most general Hamiltonian which transforms under the present RG is

$$-\beta\mathcal{K}(H,K,L,P,Q,R,C) = H \sum_i S_i + K \sum_{\langle ij \rangle} S_i S_j + L \sum_{\langle\langle ij \rangle\rangle} S_i S_j + P \sum_{\Delta} S_i S_j S_k + Q \sum' S_i S_j S_k + R \sum'' S_i S_j S_k S_l + NC \quad (2.2)$$

where the primes denote summation over the appropriate groups of spins.

The partial partition functions are now calculated in the standard fashion.¹⁵ The notation to be used is $Z(S_A, S_B, S_C, S_D)$, where this stands for the partition function calculated when the cells A , B , C , and D are constrained to have cell spins equal to

S_A , S_B , S_C , and S_D , respectively. Since the parameter space consists of seven independent interactions, including the zero-spin interaction, seven independent partial partition functions are necessary to specify them all. However, only five partition functions are independent; namely, $Z(++++)$, $Z(+++-)$, $Z(++--)$, $Z(+---)$, $Z(----)$. This results

from the fact that all the sublattices are treated equivalently, and thus, $Z(S_A, S_B, S_C, S_D)$ is invariant under arbitrary permutation of its arguments. Therefore, the only independent partition functions are simply those for which zero, one, two, three, or four cell spins are "down". As a result, all seven interaction parameters cannot be uniquely specified. In fact, the recursion relations are found to be

$$\begin{aligned} H' &= \frac{1}{16} \ln \left[\frac{Z(++++)Z^2(+++-)}{Z(-----)Z^2(+---)} \right], \\ K' + L' &= \frac{1}{32} \ln \left[\frac{Z(++++)Z(-----)}{Z^2(++--)} \right], \\ P' + 3Q' &= \frac{1}{32} \ln \left[\frac{Z(++++)Z^2(+---)}{Z(-----)Z^2(++++)} \right], \\ R' &= \frac{1}{192} \ln \left[\frac{Z(++++)Z^6(+++-)Z(-----)}{Z(-----)Z^2(++++)} \right], \\ C' &= 3C + \frac{1}{64} \ln [Z(++++)Z^4(+++-)Z^6(+++-) \\ &\quad \times Z^4(+---)Z(-----)], \end{aligned} \quad (2.3)$$

so that only the combinations $K' + L'$ and $P' + 3Q'$ can be determined, and not K', L', P' , and Q' individually. Of course in the initial Hamiltonian all interaction parameters can take on any value one may choose; only after iteration of the RG do K', L' and P', Q' lose their individual identity. Thus on subsequent iterations it is necessary to assign a relationship between K', L', P' , and Q' . As no obvious way exists to distinguish between the various two- and three-spin interactions, the simple choice $K' = L'$ and $P' = Q'$ has been used throughout. With this prescription, plus the recursion relations (2.3), we are now in a position to calculate all quantities of interest within the context of our approximate renormalization group.

C. Results

The RG developed in Sec. IIB will now be studied in detail. We begin by considering the ferromagnetic transition, for which an exact solution is known.¹⁶ The result for the critical coupling is $K_c = 0.181$ (0.275 exact), while the two relevant exponents are $\nu_H = 1.388$ (1.875 exact) and $\nu_T = 0.64$ (1.0 exact). The fact that these results are significantly smaller than the corresponding exact values is consistent with our previous experience⁵; namely, that sublattice renormalization groups of the type presented here systematically underestimate critical exponents.

Consider now the antiferromagnetic regime, that is, the Hamiltonian of Eq. (2.1) with both K and L negative (i.e., repulsive). The expected behavior for this case has been represented schematically in Fig. 2. The phase diagram which results from our RG treat-

ment is determined by the intersection of the global (H, K, L, P, Q, R) critical surfaces with the surface $K, L < 0, P = Q = R = 0$. Figure 6 shows the phase diagram for the particular case $L = K$ (note that this choice of $L = K$ for the initial Hamiltonian has no connection with the choice made above of $L' = K'$, which holds only after the first RG iteration). This phase diagram is in qualitative agreement with recent Monte Carlo simulations.¹⁷ However, significant differences do exist between the behavior found here and that which was outlined in Sec. II A. In particular, the region around $H = 0$ does not possess the lens-shaped feature shown in Fig. 2, but rather exhibits only a single transition. Furthermore, for $H = 0$ the system should exhibit a transition in the universality class of the Heisenberg model with cubic anisotropy, and for nonzero H the transition should have the critical behavior of the four-state Potts model. It follows that one would expect a fixed point at $H = 0$ which is relevant with respect to the magnetic field, and that another fixed point, possibly the same one that governs the low-density 2×2 phase, would control the transition for finite fields. A fixed point is found at $H = 0$ for this approximate RG; however it is irrelevant with respect to the field and thus governs the entire high-density phase boundary. Another fixed point is found which governs the low-density 2×2 phase. Presumably, the magnetic exponent for the $H = 0$ fixed point has been underestimated by this RG to the extent that it has become irrelevant, thus changing the qualitative appearance of the phase diagram.

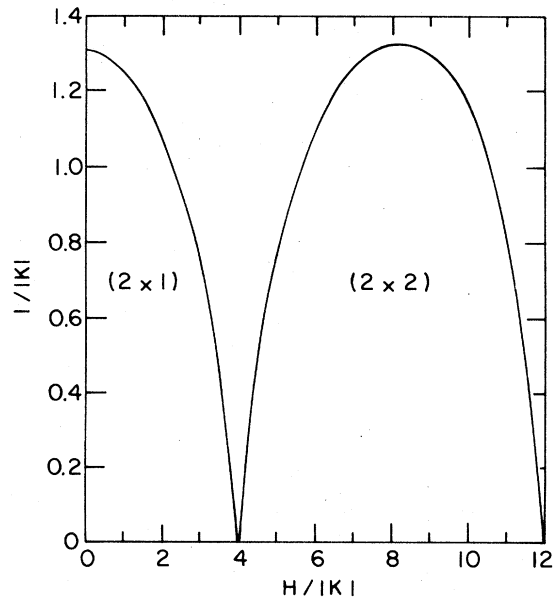


FIG. 6. Calculated phase diagram for the ratio $a=1$. The ordinate and abscissa are temperature and magnetic field.

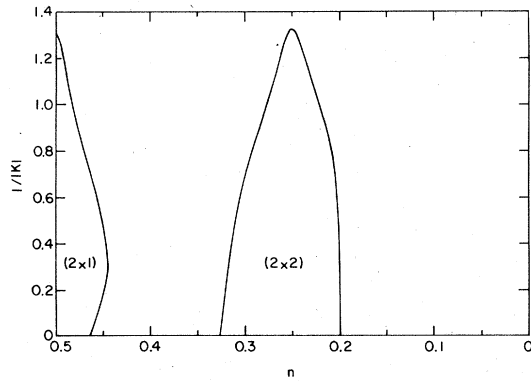


FIG. 7. Same diagram as in Fig. 6 but converted to temperature and coverage.

In Fig. 7 we have converted the phase diagram of Fig. 6 to temperature versus coverage. Note, in particular, that the 2×1 and 2×2 transitions are peaked about coverage $\frac{1}{2}$ and $\frac{1}{4}$, respectively. Also, the phase diagram is symmetric about $n = \frac{1}{2}$. The fixed point governing the 2×1 transition is located at $H^* = P^* = Q^* = 0$, $K^* = L^* = -0.341$, and $R^* = 0.145$. The relevant exponent is $y_T = 0.886$ which implies $\alpha = -0.26$. This is not too different from the value $y_T = 0.92$ calculated by Domany and Riedel.¹⁸ The heat capacity taken at $n = \frac{1}{2}$ (i.e., $H = 0$) is shown in Fig. 8. The slope of the specific heat is infinite at T_c . As the ratio of the amplitudes of the singularity above and below T_c is negative, there is no cusp.

For the 2×2 transition the fixed point occurs at zero temperature, and thus at infinite values of the

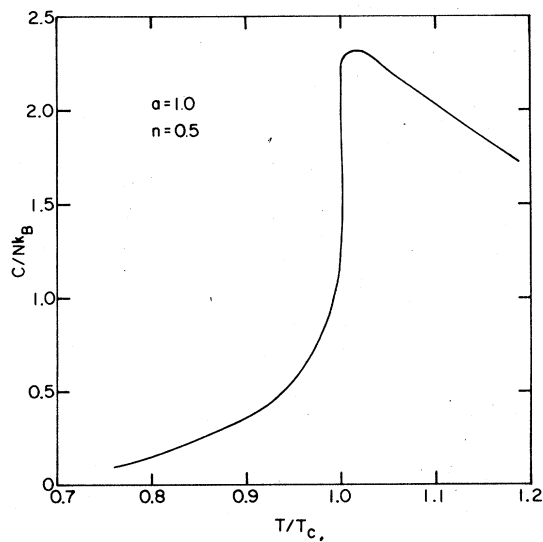


FIG. 8. Specific heat vs temperature at coverage of $\frac{1}{2}$. The ratio $a = 1$.

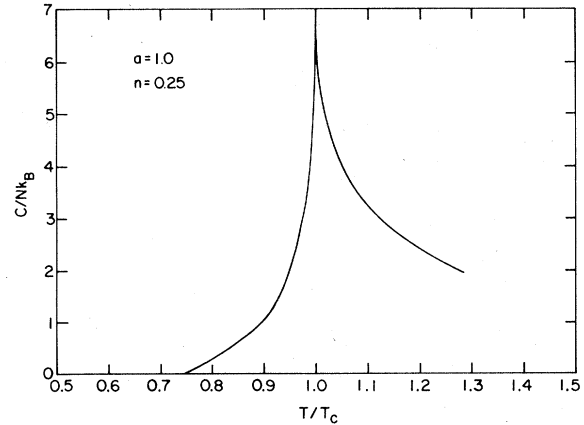


FIG. 9. Specific heat vs temperature at coverage of $\frac{1}{4}$. The ratio $a = 1$.

interaction parameters. In particular, $H^* = \pm\infty$, $K^* = L^* = -\infty$, $P^* = Q^* = \pm\infty$, $R^* = -\infty$; and these go to infinity in such a way that

$$\pm H^* + 6(K^* + L^*) \pm 6(P^* + 3Q^*) + 12R^* = \frac{1}{2} \ln\left[\frac{1}{2}(\sqrt{85} - 9)\right] \approx -1.10$$

The relevant exponent for this fixed point is $y_T = 1.03$, so that $\alpha = 0.059$. Thus the heat capacity for this transition diverges as the temperature approaches T_c . In Fig. 9 the heat capacity at $n = \frac{1}{4}$ is shown. The value of α expected for the 2×2 transition is that of the four-state Potts model, which is believed¹⁹ to be $\alpha = \frac{2}{3}$. Here, again, we see that our sublattice RG greatly underestimates the critical exponents of the system.

Finally, while investigating this model for $L = K$ is instructive, we do not expect physical systems to be well described by this condition. In fact, for phy-

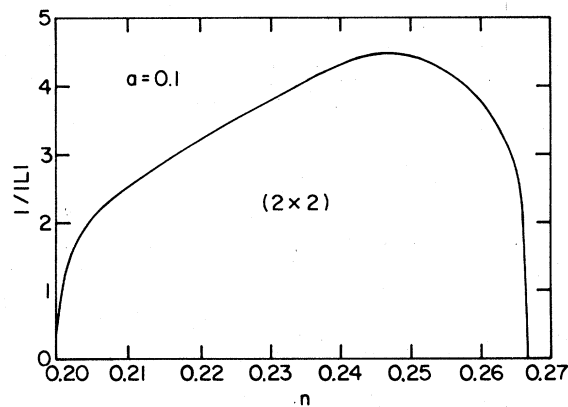


FIG. 10. Region of existence of the 2×2 phase on the triangular lattice for $a = 0.1$. The region of existence for infinite nearest-neighbor repulsion, $a = 0$, is the same.

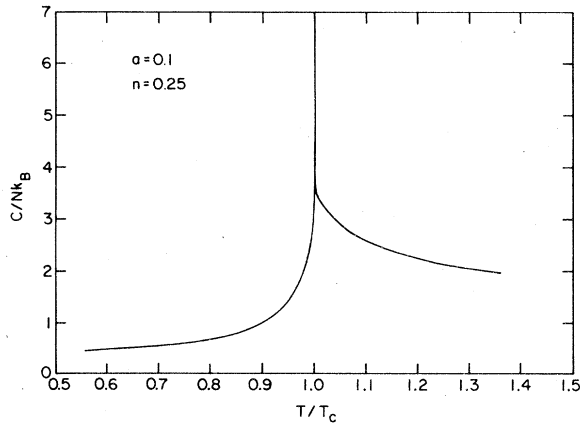


FIG. 11. Specific heat vs temperature at coverage of $\frac{1}{4}$. The ratio $a = 0.1$.

isorbed systems we expect that $K \gg L$, and thus we investigate our recursion relations for the limit in which $a = L/K$ tends to zero. As a practical matter, we find that calculations for $a = 0.1$ are sufficient to yield the limiting behavior as $a \rightarrow 0$. We now consider some results from our RG for $a = 0.1$. First, since $K \gg L$ it will be extremely unfavorable for nearest-neighbor sites to be occupied, and thus the coverage will not easily exceed one-third. Therefore, the 2×1 transition will not be seen, and so, in Fig. 10, we show the 2×2 transition for $a = 0.1$. Note the small range in coverage over which the transition is observed, and also that the temperature scale is now given by $1/|L|$. Second, in Fig. 11, we display the heat capacity taken at a constant coverage $n = \frac{1}{4}$. Extremely close to the peak the specific heat must be poor due to our incorrect exponent. It is hoped that, as in our previous calculation, the results away from T_c are rather good.

III. 2×2 TRANSITION ON THE HONEYCOMB LATTICE

In order to study the transition to the nonprimitive 2×2 state of the honeycomb lattice shown in Fig. 12 we consider a lattice gas with first- and second-neighbor repulsions of strengths u_1 and u_2 . The problem maps onto the Ising model with the same reduced Hamiltonian as in Eq. (2.1). The sole difference is that a site on the honeycomb lattice has only three nearest neighbors instead of the six of a triangular lattice. This is reflected in the expressions for the magnetic field and the constant term which now read

$$H = \frac{1}{2} [\beta\mu - \frac{3}{2}\beta(u_1 + 2u_2) - \ln \lambda_7^2 / v_0] ,$$

$$C = \frac{1}{2} [\beta\mu - \frac{3}{4}\beta(u_1 + 2u_2) - \ln \lambda_7^2 / v_0] .$$

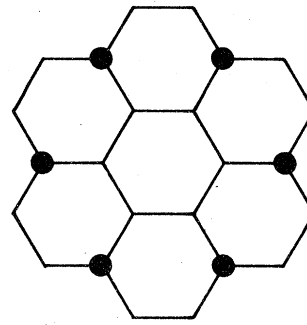


FIG. 12. Nonprimitive 2×2 structure on the honeycomb lattice.

As before, the reduced interactions, $K = -\frac{1}{4}\beta u_1$ and $L = -\frac{1}{4}\beta u_2$, are negative.

The honeycomb lattice consists of a triangular Bravais lattice with a basis of two sites per unit cell. It is desirable to exploit this relationship and construct an RG very much like the one described in Sec. II B. We do this by carrying out a prefacing transformation which maps the original system on the hexagonal lattice to a renormalized system on a triangular lattice. Once this has been done the RG of Sec. II B can be used to carry out subsequent iterations.

To construct the prefacing transformation we divide the hexagonal lattice into four sublattices, shown in Fig. 13. Cells are now chosen to consist of two spins both from the same sublattice and represented by a dashed line in Fig. 13. Each sublattice is treated equivalently and the total sublattice symmetry is preserved. Furthermore, the cell spins form the same diamond-shaped configuration displayed by the cell spins in our triangular lattice RG of Sec. II. Thus, performing one iteration of this prefacing transformation will map the hexagonal lat-

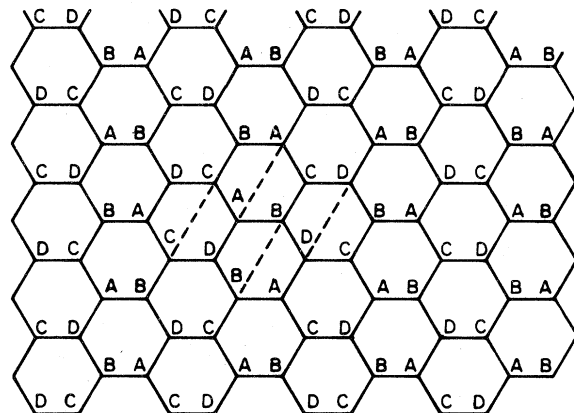


FIG. 13. Division of the honeycomb lattice into four sublattices. The sites are grouped into cells of two sites from one sublattice. Dotted lines connect sites in the same cell.

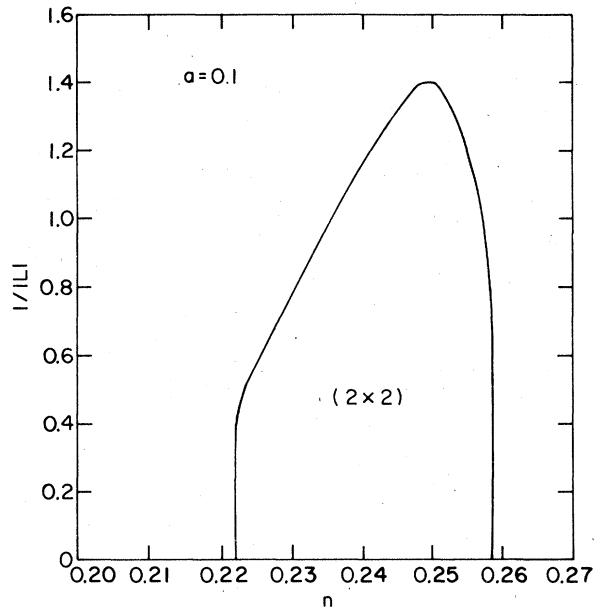


FIG. 14. Region of existence of the nonprimitive 2×2 phase on the honeycomb lattice for $a=0.1$. The region of existence for infinite nearest-neighbor repulsions, $a=0$, is the same.

tice onto the triangular lattice, and in so doing, generate the same set of interaction parameters as before. Further, the 2×2 state of Fig. 12 is mapped onto the 2×2 state of the triangular lattice.

For the prefacing transformation eight spins are used, and these are considered to be periodically extended over the lattice, as are the cell spins. Again, the cell-cluster method of Niemeijer and van Leeuwen is employed. The most general projection operator for a two-spin cell can be written

$$p(S'; S_1, S_2) = \frac{1}{2} [1 + u(S_1 + S_2)S'] ,$$

in which S_1, S_2 are the site spins and S' is the cell spin. The choice used here is $u = \frac{1}{2}$, corresponding to majority rule with the following proviso; if the sum of S_1, S_2 is zero for a given state, then it is projected equally onto $S' = \pm 1$. Using this projection the partial partition functions can now be calculated. Just as for the triangular system, only five partition functions, $Z(++++)$, $Z(+++-)$, $Z(++--)$, $Z(+---)$, $Z(----)$, are independent. Moreover, since the cell spins are in exactly the same array as in Sec. II, the renormalized couplings are again given by Eqs. (2.3). So, Eqs. (2.3) are used on each iteration, the difference is that the partition functions used for the first step (the prefacing transformation) will be different from those employed in subsequent steps.

Fixed points and exponents are, of course, those of Sec. II B. Thus universality has been incorporated in a trivial way. Nonuniversal features do differ because of the different first step.

The parameter range of physical interest is presumably that for which the nearest-neighbor repulsion is very large so that $a = L/K$ is vanishingly small. By examining the phase diagram in temperature (in units of the second-neighbor interaction) versus coverage, we find that there is little change for values of a smaller than 0.1. The diagram for this value of a is shown in Fig. 14 for coverages near $\frac{1}{4}$. Note that coverages beyond $\frac{1}{3}$ are inaccessible, and the coverage range over which the phase exists is very narrow. It is interesting to note that a continuous transition to some 2×2 state in the system O on Ni(111) was recently reported to occur in a very narrow coverage range.¹¹ Conversely, we have recently argued²⁰ that the broad coverage range over which a transition to the 2×2 state of Fig. 14 occurs in H on Ni(111) indicates the presence of third-neighbor attractions in that system.

IV. SUMMARY

The transition to a 2×2 structure on the triangular lattice is in the particularly interesting class of the four-state Potts model. We have studied a simple model which displays this transition; the triangular lattice gas with repulsive first- and second-neighbor interactions. Qualitative features of the expected phase diagram were extracted from symmetry and ground-state energy arguments. A position-space RG calculation was then employed which preserved the symmetry of the 2×2 structure. The resulting phase diagram has deficiencies in density regimes other than the one in which we are interested. In that regime it would appear to be an adequate approximation. A simple extension of the RG permitted calculation of the boundary of the analogous phase on the honeycomb lattice. Results for the physically interesting regime of large first-neighbor repulsion are shown for the triangle and honeycomb in Figs. 10 and 14.

ACKNOWLEDGMENTS

We would like to thank J. G. Dash, E. Domany, S. C. Fain, E. K. Riedel, and O. E. Vilches for numerous discussions, and Mr. P-L. Lee for assistance in the computations. This work was supported by the NSF under Grant No. DMR 73-02582 A02.

- ¹E. Domany, M. Schick, J. S. Walker, and R. B. Griffiths, *Phys. Rev. B* **18**, 2209 (1978).
- ²S. Alexander, *Phys. Lett. A* **54**, 353 (1975).
- ³M. Bretz, *Phys. Rev. Lett.* **38**, 501 (1977).
- ⁴P. M. Horn, R. J. B. Birgeneau, P. Heeney, and E. M. Hammonds, *Phys. Rev. Lett.* **41**, 961 (1978).
- ⁵M. Schick, J. S. Walker, and M. Wortis, *Phys. Rev. B* **16**, 2205 (1977).
- ⁶A. N. Berker, S. Ostlund, and F. A. Putnam, *Phys. Rev. B* **17**, 3650 (1978).
- ⁷S. Ostlund and A. N. Berker, *Phys. Rev. Lett.* **42**, 843 (1979).
- ⁸T. B. Grimley and S. M. Walker, *Surf. Sci.* **14**, 406 (1969).
- ⁹P. Pfeuty and G. Toulouse, *Introduction to the Renormalization Group and to Critical Phenomena* (Wiley, New York, 1975), p. 141.
- ¹⁰E. Domany, M. Schick, and J. S. Walker, *Phys. Rev. Lett.* **20**, 1148 (1977).
- ¹¹A. R. Kortan, P. I. Cohen, and R. L. Park (unpublished).
- ¹²M. A. Van Hove, G. Ertl, K. Christmann, R. J. Behm, and W. H. Weinberg, *Solid State Commun.* (to be published).
- ¹³L. D. Landau and E. M. Lifshitz, *Statistical Physics*, 2nd ed. (Pergamon, New York, 1968), Chap. XIV.
- ¹⁴J. M. J. van Leeuwen, *Phys. Rev. Lett.* **16**, 1056 (1975).
- ¹⁵Th. Niemeijer and J. M. J. van Leeuwen, *Physica (Utrecht)* **71**, 17 (1974).
- ¹⁶R. M. F. Houtappel, *Physica (Utrecht)* **16**, 425 (1950).
- ¹⁷D. P. Landau (private communication).
- ¹⁸E. Domany and E. K. Riedel, *Phys. Rev. B* **19**, 5817 (1979).
- ¹⁹Because the four-state Potts and the Baxter-Wu model have identical Landau-Ginzburg-Wilson Hamiltonians to lowest order, they are believed to have the same exponents. The Baxter-Wu exponent is known exactly. R. J. Baxter and F. Y. Wu, *Phys. Rev. Lett.* **31**, 1294 (1973).
- ²⁰E. Domany, M. Schick, and J. S. Walker, *Solid State Commun.* (to be published).